12

# Polarization-Selective Substrate-Mode Volume Holograms and Its Application to Optical Circulators

Jing-Heng Chen[1], Kun-Huang Chen[1] and Der-Chin Su[2]
[1]*Feng Chia University*
[2]*National Chiao Tung University*
*Taiwan*

## 1. Introduction

Optical circulators [Ramaswami et al., 2009; Hecht, 2005; Mynbaev & Scheiner, 2000] are important nonreciprocal devices that can direct a light from one port to another in only one direction. They are essential components in the construction of fundamental network modules, such as optical add–drop multiplexers, dispersion-compensation, optical amplifiers, and time-domain reflectometry. Different kinds of design of optical circulator have been proposed [Iwamura et al., 1979; Shirasaki et al., 1981; Yokohama et al., 1986; Koga, 1994; Wang, 1998]. According to the operation principles, optical circulators can be divided into three types, traditional, waveguide, and holographic. The traditional optical circulators mainly apply spatial walk-off polarizers (SWPs) [Nicholls, 2001], Faraday rotators (FRs), and half-wave plates (Hs) to implement its function. The waveguide optical circulators utilize a waveguide Mach–Zehnder interferometer to implement the function of SWPs. The holographic optical circulators apply holographic optical elements to replace traditional SWPs. Accordingly, the spatial walk-off polarizer is a key component in the design of optical circulator that significantly influences the performances and cost of a device.

Traditional spatial walk-off polarizers are essentially birefringent crystals that can split an optical beam into two orthogonally polarized beams. However, birefringent crystals suffer from challenges of highly optical qualities, crystal manufacturing, and hard optical fabrications. The highly optical qualities mean high transparency and optical uniformity for a wide spectrum range, high birefringence, and enough hardness. The main crystal growth thechnologies are Czochralski method and Verneuil process. The hard fabrications include x-ray orientation, slicing, polishing, coating, cleaning, testing, packaging, and related processes. Therefore, the cost is hard to down. In addition, limited by the finite birefringence, the beam splitting distance is small. Therefore, the device length is hard to shorted.

Compare to the crystal-type SWPs, polarization-selective substrate-mode volume holograms (PSVHs) [Huang, 1994] have a large splitting angle and several superior advantages. A PSVH are phase volume holograms stacked on a glass or plastic substrate and signals transmit in the substrate by total internal reflection. With this planar structure, PSVHs have advantages of easy fabrication, low cost, high efficiency, compactness, easy coupling, and easily to combine with other elements. Due to these merits, PSVHs had been widely applied

in several optical systems, such as optical sensing, optical data storage, imaging system, and switching network. In 2003, the PSVHs was firstly proposed to replace crystal-type SWPs in a four-port optical ciculator [Chen et al., 2003]. In the application, these PSVHs are consequently termed as holographic spatial walk-off polarizer (HSWP). Due to the introduction of HSWPs, the fabricated four-port optical circulator has advantages of polarization-independence, compactness, high isolation, low polarization mode dispersion, low cost, and easy fabrication.

However, the feasibility of conventional PSVHs is usually limited by the finite refractive index modulation strength of a recording material. The common solution is to increase the thickness of the recording material, in order to compensate the shortage of the refractive index modulation strength in the phase modulation term. However, under the thickness condition of thick material, the distortion effect of interference fringe is worsened. An ideal holographic recording condition hinges on the thin thickness of a recording material with a high refractive index modulation strength. Actually these cannot be completed in both respects. To overcome the problems, based on the coupled-wave theory and the structure of substrate-mode hologram, a special design of PSVHs was proposed with a relatively large splitting angle near 90° [Chen et al., 2008]. With this design, a low refractive index modulation strength is required, which can be easily achieved with common recording materials. In addition, this design should bear all merits of conventional PSVHs.

As the design of optical communication systems becomes more and more complex, an optical circulator with many input and output ports has become highly desirable. However, the port numbers for presently most commercial optical circulators are limited. In 2004, based on holographic spatial- and polarization-modules (HSPMs), two kinds design of holographic-type multi-port optical circulator were also proposed [Chen et al., 2004; Chen et al., 2004]. The HSPM is consisted of two HSWPs, an half-wave plate (H), and a Faraday rotator (FR). The merits of these designs include polarization-independence, compactness, high isolation, low polarization mode dispersion, and easy fabrication. Furthermore, the number of port can be scaled up easily.

Accordingly, this chapter devotes to introduce the polarization-selective substrate-mode volume hologram in several respects and its novel applications in design of optical circulator. The second section, according to coupled-wave theory, will clearly describe the principle and characteristic of conventional PSVHs; a modified design method of PSVHs will also be described to overcome the shortage in refractive index modulation strength. The third section will introduce the applications of PSVH to optical circulators. The principle and operation characteristic of a four-port optical circulator will be introduced. The following context will introduce the principles and operation characteristic of holographic spatial- and polarization-modules (HSPMs) and their applications to multi-port optical circulators. All the design details will be described and their characteristic will be discussed. Finally, the fourth section is conclusion.

## 2. Polarization-selective substrate-mode volume holograms

### 2.1 Conventional polarization-selective substrate-mode volume holograms

Figure 1 shows the structure of the conventional polarization-selective substrate-mode hologram [Huang, 1994] which is composed of four volume holograms, input grating coupler ($H_I$), polarization beam splitter hologram ($H_{PBS}$), output grating couplers ($H_{OS}$ and $H_{OP}$), and two substrates. An unpolarized light is incident on $H_I$ normally, and is diffracted

into $H_{PBS}$ at a special angle. The output diffraction lights of $H_{PBS}$ are split into *s*- and *p*-components which are perpendicular to each other. These two components are then total internal reflected (TIR) at the base of the substrate and are diffracted and coupled out normally by $H_{OS}$ and $H_{OP}$, respectively. Therefore, the *s*- and *p*-polarized lights are successfully separated.

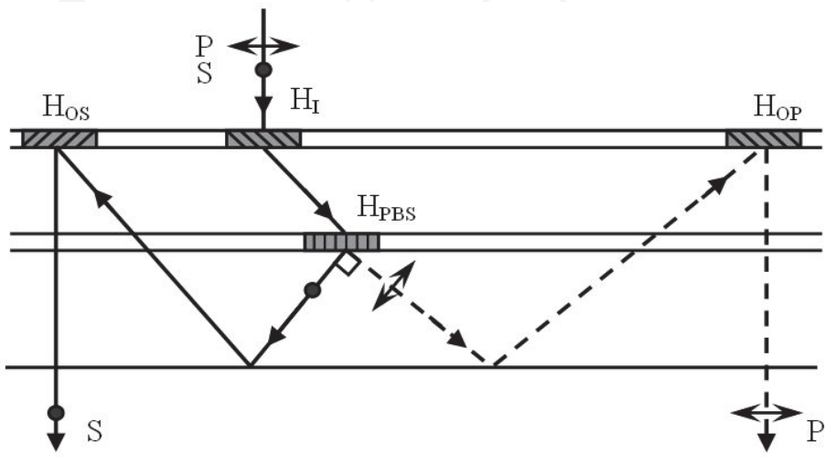


Fig. 1. Schematic representation of the conventional polarization-selective substrate-mode volume hologram.

In this structure, $H_I$, $H_{PBS}$, $H_{OS}$, and $H_{OP}$ are actually transmission-type phase volume holograms and can be designed according to the coupled-wave theory [Kogelnik, 1969]. For a transmission-type phase volume hologram, as shown in Fig. 2, the relation between the diffraction efficiencies of *s*- and *p*-components can be written as

$$\eta_{s,p} = \sin^2 \upsilon_{s,p}, \tag{1}$$

where the modulation parameters for *s*- and *p*-components, $\upsilon_s$ and $\upsilon_p$, are given as

$$\upsilon_s = \frac{\pi N_1}{(\cos\theta_{r1}\cos\theta_{r2})^{1/2}}, \tag{2}$$

$$\upsilon_p = \upsilon_s \cos(\theta_{r2} - \theta_{r1}), \tag{3}$$

and

$$N_1 = \frac{n_1 d}{\lambda}. \tag{4}$$

$N_1$ is the effective index modulation in which $\lambda$ is the reconstruction wavelength, $d$ is the thickness of the recording material, and $n_1$ is the refractive index modulation. $\theta_{r1}$ and $\theta_{r2}$ are corresponding angles of the reconstruction and the diffraction beams in the recording material, respectively.

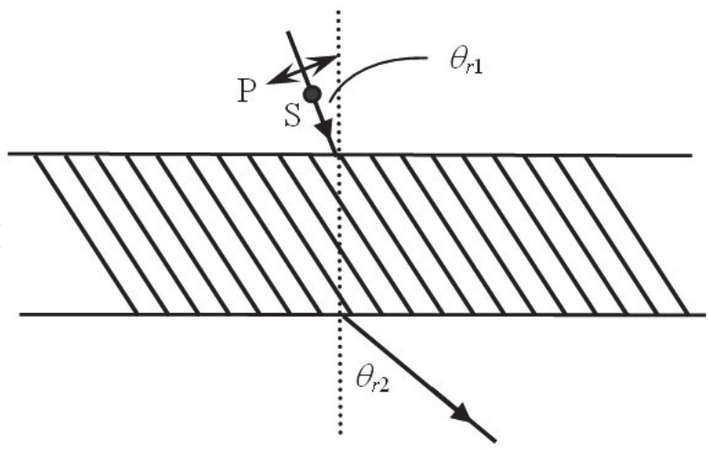


Fig. 2. Reconstruction geometry of the phase volume hologram: S, *s*-polarization field; P, *p*-polarization field.

In the case of normal incident, *i.e.* $\theta_{r1}$=0°, eqs. (2) and (3) can be reduced as

$$\upsilon_s = \frac{\pi N_1}{\left(\cos\theta_{r2}\right)^{1/2}}, \tag{5}$$

$$\upsilon_p = \upsilon_s \cos\left(\theta_{r2}\right). \tag{6}$$

Accordingly, the design of $H_I$ requires $\eta_s=\eta_p\geq 90\%$ that can be solved by eqs. (1)-(6). The function of $H_{PBS}$ requires $\eta_s$=100% and $\eta_p$=0 or $\eta_s$=0 and $\eta_p$=100%. The functions of $H_{OP}$ and $H_{OS}$ require $\eta_p$=100% ($\eta_s$=0) and $\eta_s$=100% ($\eta_p$=0), respectively.

However, in order to satisfy the requirements of $H_{OP}$ and $H_{OS}$, the parameters $\upsilon_s$ and $\upsilon_p$ stand on the following conditions: (1) $\upsilon_s=[m+(1/2)]\pi$ and $\upsilon_p=m\pi$ (for $\eta_s$=100% and $\eta_p$=0); (2) $\upsilon_s=m\pi$ and $\upsilon_p=[m-(1/2)]\pi$ (for $\eta_s$=0 and $\eta_p$=100%), where $m$ is a positive integer. Under these conditions, the values of related parameters $m$, $\theta_{r2}$, and $N_1$ are listed in Table 1. In order to fulfill the required TIR inside the substrates, only conditions at $m$=1 are valid. However, the feasibility of fabricating these elements is usually limited by the finite refractive index modulation strength $n_1$ of a recording material. Therefore, an alternative design method is described below to overcome this drawback.

| | | *m* | | | | |
|---|---|---|---|---|---|---|
| | | 1 | 2 | 3 | 4 | 5 |
| $\theta_{r2}$ | Condition (1) | 48.2° | 36.9° | 31.0° | 27.3° | 24.6° |
| | Condition (2) | 60.0° | 41.4° | 33.5° | 29.0° | 25.8° |
| $N_1$ | Condition (1) | 1.22 | 2.24 | 3.24 | 4.24 | 5.24 |
| | Condition (2) | 0.707 | 1.73 | 2.74 | 3.74 | 4.74 |

Table 1. Related parameters for condition (1) ($\eta_s$=100% and $\eta_p$=0) and condition (2) ($\eta_s$=0 and $\eta_p$=100%).

### 2.2 Alternative design of polarization-selective substrate-mode volume holograms

Shown in Fig. 3 is a schematic representation of the proposed polarization-selective substrate-mode volume hologram [Chen et al., 2008] which is consisted of a transmission-type phase volume holographic grating and a substrate. Its grating structure is designed in such a way that either of the *s*- or *p*-polarized component of a normal incident beam at A is transmitted straight through the grating and the substrate (channel 1) while the other orthogonally polarized component is completely diffracted into the substrate with a large diffraction angle $\theta_{r2}$ which is larger than the critical angle $\theta_c$ at the interface of recording material and substrate. In this way, the diffracted beam is totally reflected at point B and hits the grating again at point C. This beam is totally reflected at point C, and the reflected beam from point C satisfies the Bragg condition of the grating. The propagation direction of the reflected beam is in parallel to that of the beam diffracted by the grating at point A. Because the structure of the grating at point C is the same as that at point A, the diffracted beam at point C will be in parallel to the input beam at point A; that is, the output beam passes normally through the substrate (channel 2). The detail of the beam propagation at point C is shown in the upper right circle of Fig. 3. Consequently, two orthogonally polarized parallel beams with the separation of length AC=2$d$(tan$\theta_{r2}$) can be obtained in which $d$ is the thickness of the recording material.

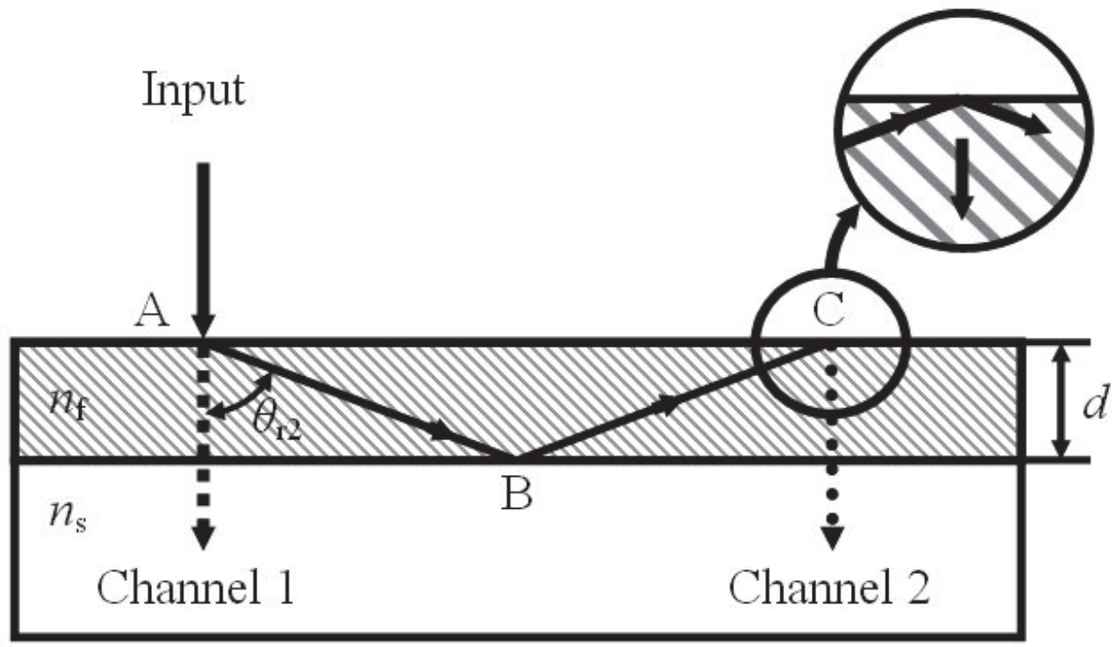


Fig. 3. Schematic representation of the proposed polarization-selective substrate-mode volume hologram (I).

In addition, in the same principle, we can properly choose the substrate with its refractive index equally that of the recording material ($n_s$=$n_f$). Under this condition, the light propagation details in Fig. 3 change as shown in Fig. 4. The light separated distance becomes AC=2$t$(tan$\theta_{r2}$) in which $t$ is the thickness of the substrate. In generally, the structure in Fig. 3 is suitable for integrated optical systems, and that in Fig. 4 can be applied in common optical systems for the purpose of more compactness.

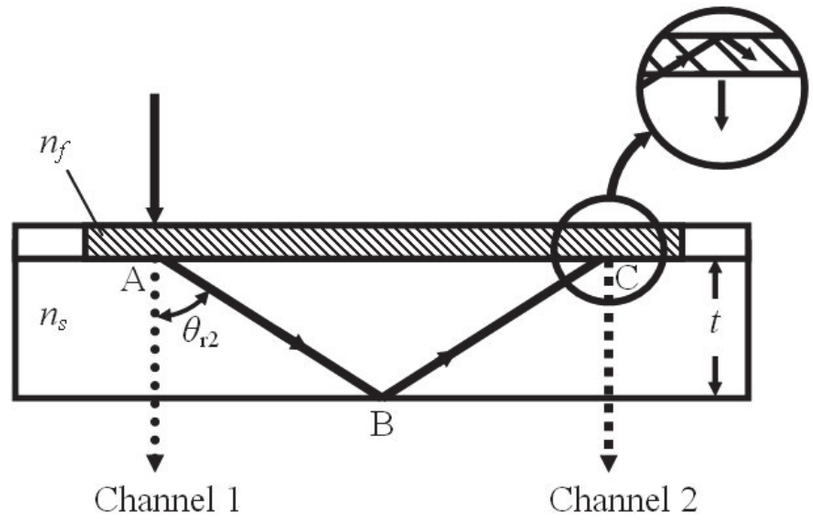


Fig. 4. Schematic representation of the proposed polarization-selective substrate-mode volume hologram (II).

According to eqs. (1), (5), and (6), the relation between the diffraction efficiencies of *s*- and *p*-components can be rewritten as

$$\eta_s = \sin^2(\frac{x}{a}), \tag{7a}$$

and

$$\eta_p = \sin^2(ax), \tag{7b}$$

where

$$x = \frac{\pi n_1 d}{\lambda}, \tag{8a}$$

and

$$a = (\cos\theta_{r2})^{1/2}. \tag{8b}$$

It is obvious from eqs. (7a) and (7b) that the diffraction efficiencies of *s*- and *p*- components oscillate in the form of a sine square function asynchronously of which the primitive periods are $T_s=a\pi$ and $T_p=\pi/a$, respectively. Therefore, when $\theta_{r2}$ has a large diffraction angle near 90°, the parameter $a$ has a relative small value. This condition results a smaller value of $T_s$ and a larger value of $T_p$, and the peak values of *s*- and *p*- diffraction efficiencies leave far away each other. The smaller value of $T_s$ means a smaller required phase modulation. Therefore, in the condition of a small phase modulation value $n_1d$, we can obtain a desired result of $\eta_s$=100% and $\eta_p$~0 and complete the purpose of polarization beam splitting effectively. Shown in Fig. 5 is the relation of diffraction efficiencies v.s. $x$ considering $\theta_{r2}$=85°. It is obviously that when the value of $x$ equals 0.46, corresponding to an effective index modulation $N_1$=0.15, we can obtain $\eta_s$=100% and $\eta_p\cong$1.89%.

Shown in Fig. 6 is a preliminary measurement result of a fabricated element for *p*-polarized input signal. The thickness $t$ of the substrate is 1.50mm, and the light separating distance is about 26mm. The technique of shorter wavelength construction for longer wavelength reconstruction is applied for the fabrication of the holographic polarization selective element. A 532nm solid-state laser was applied as the exposure light source. Silver-halide recording material (VRP-M, Slavich) is used for the fabrication of this element designed with $\theta_{r2}$=83.5° for 632.8nm. The related recording material parameters of $n$ and $d$, before and after post-processing are measured by an optical thin film analysis system (Model: nkd-6000™, aquila Instruments Ltd.) The measured parameters are $n_{f1}$=1.60 (@ 532nm), $n_{f2}$=1.66 (@ 632.8nm), $d_1$=5.70μm, and $d_2$=5.35μm. Therefore, the ideal value of phase modulation $n_1 d$ is 0.11μm. In addition, in order to easy the operation, a right-angle prism with specification of 150×150×50mm is introduce for the exposure light guiding. Some castor oil (n=1.48, @20°C) is used as index-matching oil. Due to the large diffraction angle, a BaSF2 glass substrate ($n_s$=1.66, Producer: Schott Glaswerke and Schott Glass Technologies) with the same refractive index of recording material is used avoiding the reflection at the interface of recording material and substrate.

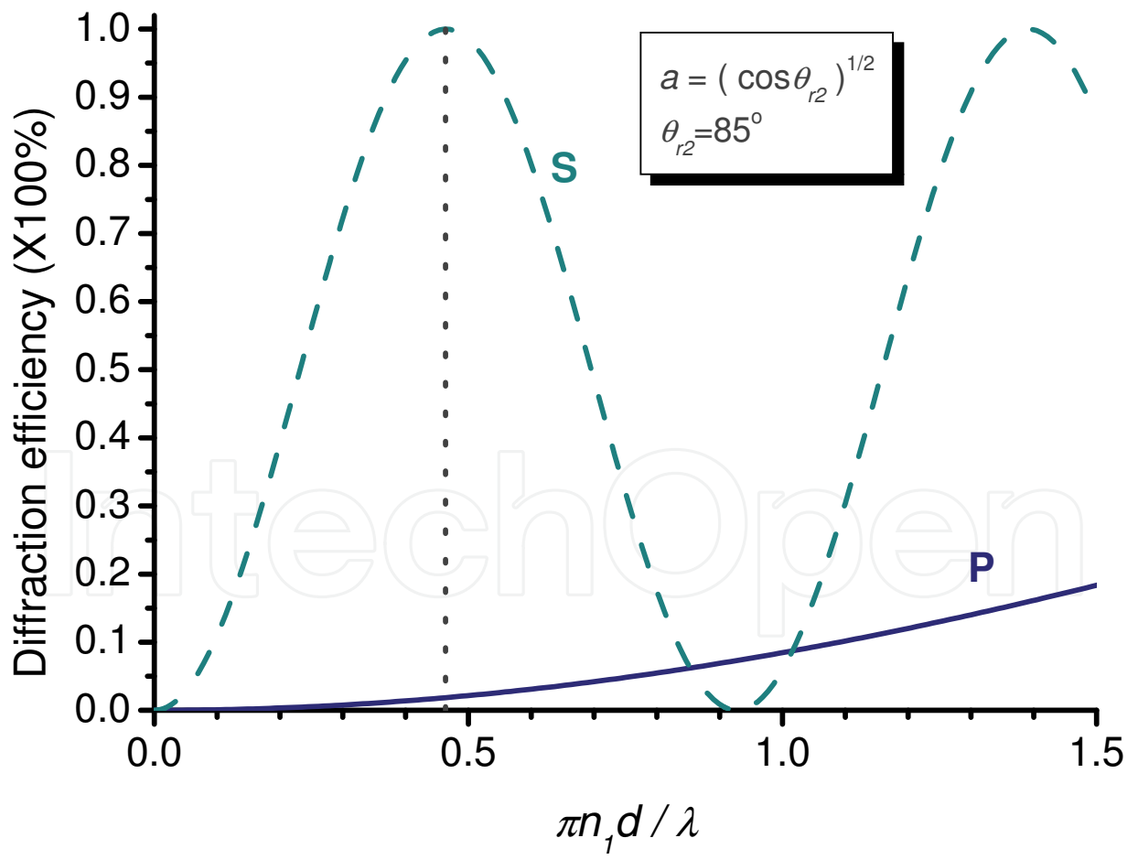


Fig. 5. The relation of $x$ v.s. diffraction efficiencies, $\eta_s$ and $\eta_p$, considering $\theta_{r2}$=85°.

Fig. 6. Transmission image for *p*-polarized input signal.

In fabrications, the value of refractive index modulation $n_1$ relates the exposure time. Therefore, according to eqs. 8(a) and 8(b), knowing the reconstruction wavelength, the recording material thickness, and the diffraction angle, the refractive index modulation $n_1$ can be obtained

$$n_1 = \frac{T_s}{2} = \frac{\lambda(\cos\theta_{r2})^{1/2}}{2d}. \tag{9}$$

In the previously mentioned case, the estimated refractive index modulation $n_1$ is 0.02 that can be obtained by controlling the exposure time experimentally.
In addition, according to eqs. (7a) and (7b), the extinction ratio (ER) of channel 1 and channel 2 can be defined as

$$ER_1 = \frac{1-\eta_p}{1-\eta_s}, \tag{10a}$$

and

$$ER_2 = \frac{\eta_s^{\,2}}{\eta_p^{\,2}} = \left[\sin(\frac{\pi\cos\theta_{r2}}{2})\right]^{-4}. \tag{10b}$$

According to eq. (10a), $ER_1$ >>1 can be obtained easily with this design. From eq. (10b), it is obvious that $ER_2$ is related with the diffraction angle $\theta_{r2}$. Therefore, $ER_2$ has a lager value as $\theta_{r2}$ is larger. Shown in Fig. 7 is the relation of $ER_2$ v.s. $\theta_{r2}$. It can be seen that the value of $ER_2$ is larger than 1000, when $\theta_{r2}$ is larger than 83.5°. In the same mentioned case, the diffraction efficiencies of the *s*- and *p*-components are about 83% and 5%, and the calculated extinction ratio of channel 1 and channel 2 are 5.58 and 275, respectively. The preliminary experimental results show the validity of the proposed method. The experimental errors mainly come from the optical setup, the process of optical exposure, and the post-processing.
In addition, the conventional polarization-selective substrate-mode volume holograms are designed with $\theta_{r2}$=48.19° and 60°. The comparisons of the improved method and conventional method are listed in Table 2. Considering the commercial holographic recording materials, the maximum values of refractive index modulation of dichromated

gelatin and silver-halide material are not excess 0.08 and 0.03, respectively. Therefore, the condition of finite phase modulation $n_1 d$ will cause these elements hard to be realized by conventional method. This situation is especially serious in the near infrared for optical communications. The improved method not only can solve the problem but also has all merits of conventional substrate-mode volume holograms such as compactness, plane structure, easily light collimation, easily fabrication, and low cost.

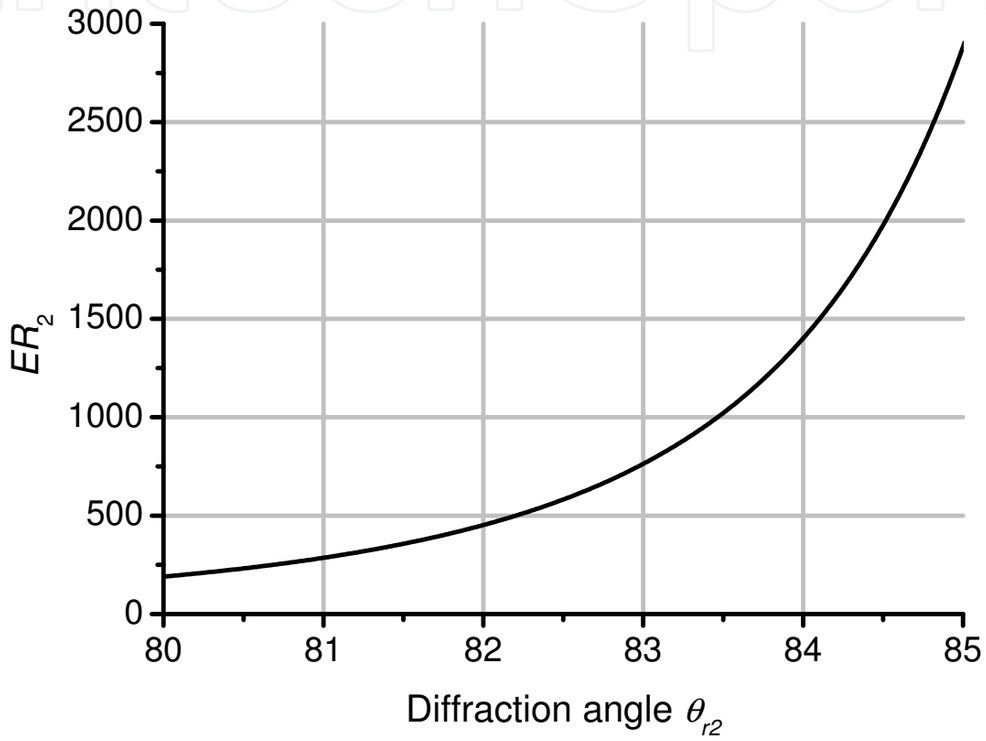


Fig. 7. The theoretical relation of $ER_2$ v.s. $\theta_{r2}$.

| | Conventional method | | | | Improved method | |
|---|---|---|---|---|---|---|
| $\theta_{r2}$ | 48.19° | | 60° | | $\theta_{r2}$ | |
| $(\eta_s, \eta_p)$ | (100%, 0) | | (0, 100%) | | $(\eta_s, \eta_p)$ | |
| $n_1 d/\lambda$ | 1.22 | | 0.71 | | $n_1 d/\lambda$ | |
| Maximum index modulation strength | $n_{DCG}$<0.08 | $n_{SH}$<0.03 | $n_{DCG}$<0.08 | $n_{SH}$<0.03 | $n_{DCG}$<0.08 | $n_{SH}$<0.03 |
| Satisfied thickness $d/\lambda$ | >15.31 | >40.82 | >8.84 | >23.57 | >1.85 | >4.92 |

Table 2. Comparisons for the improved method and conventional method; $n_{DCG}$ : maximum index modulation strength of DCG; $n_{SH}$ : maximum index modulation strength of silver-halide material.

## 3. Holographic-type optical circulators

### 3.1 Spatial- and polarization-modules

As shown in figure 8, the spatial- and polarization- module (SPM) is composed of two spatial walk-off polarizers (SWPs), a 45° Faraday rotator (FR), and a 45° half wave-plate (H). For easy understanding, an orthogonal *x*-*y*-*z* coordinate is introduced, symbol ⊕ represent an unpolarized light, and symbols ⊖ and ⏀ represent *h*-polarized (*y*-polarized) and *v*-polarized (*x*-polarized) lights, respectively.

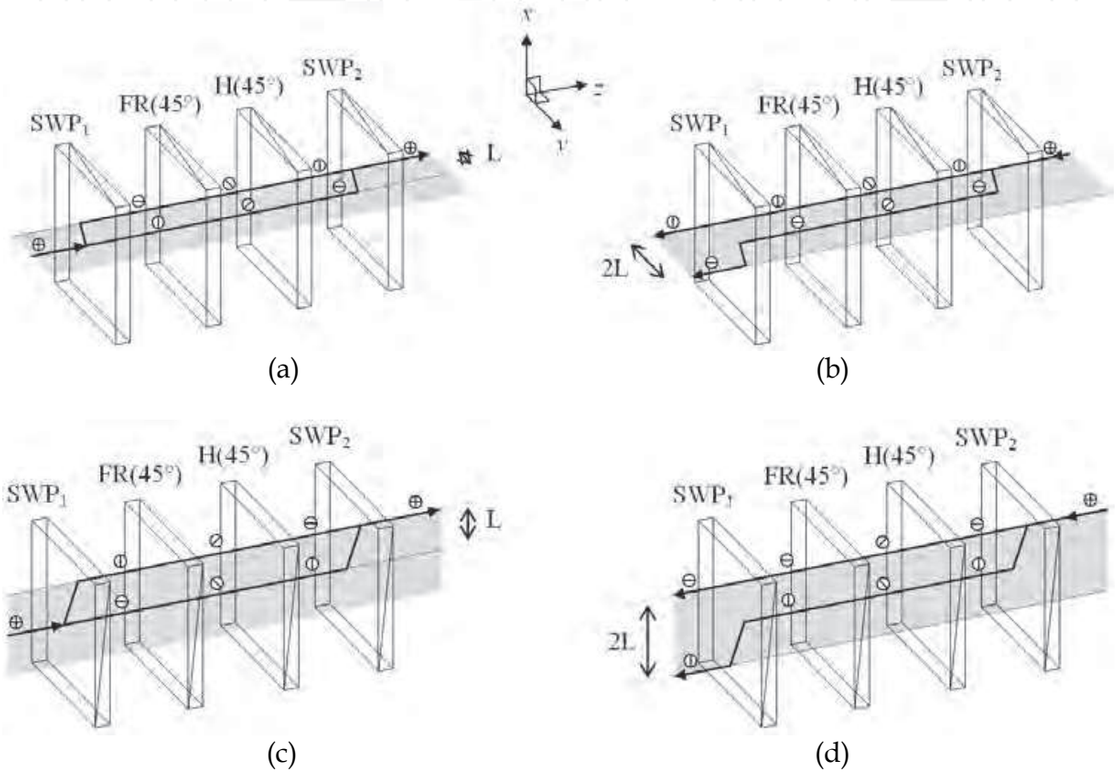


Fig. 8. Structure and operation characteristic for (a), (b) $SPM_y$ and (c), (d) $SPM_x$.

From figure 8(a), when an unpolarized light is incident into the $SWP_1$ in +*z* direction, the transmitted light is divided into two orthogonally polarized components, *h*- and *v*-polarized lights, respectively. These two lights then pass through the 45° FR and 45° H. Therefore, their statuses of polarization (SOPs) are rotated 90° in total. Continuing their journey, they enter the $SWP_2$ and are recombined together with a lateral shift *L* in −*y* direction. On the other hand, Fig. 8(b) shows that when an unpolarized light is incident into the $SWP_2$ in −*z* direction, the transmitted light is similarly divided into two orthogonally polarized components, *v*- and *h*-polarized lights. These two lights then sequentially pass through the same H and FR. Their SOPs are rotated −45° by the H and +45° by the FR. Because Faraday rotator is a nonreciprocal element, their SOPs are rotated 0° in total. Therefore, the *v*-polarized light transmits the $SWP_1$ directly and the *h*-polarized light transmits the $SWP_1$ with a lateral shift 2*L* in +*y* direction. In Figs. 8(a) and 8(b), because the shifts of transmitted light of the SPM are in *y*-direction, this operation type SPM is defined as $SPM_y$. Based on the same principle, when the $SPM_y$ is clockwise rotated

90° with respect to +$z$ axis (viewing from $SWP_1$ to $SWP_2$), the shifts of transmitted light of the SPM are in $x$-direction, as shown in Figs. 8(c) and 8(d). Accordingly, this operation type SPM is defined as $SPM_x$.

### 3.1.1 Parallel connection of two SPMs

As shown in figures 9(a) and 9(b), two $SPM_x$s are connected, *i.e.* parallel connection of two SPMs.

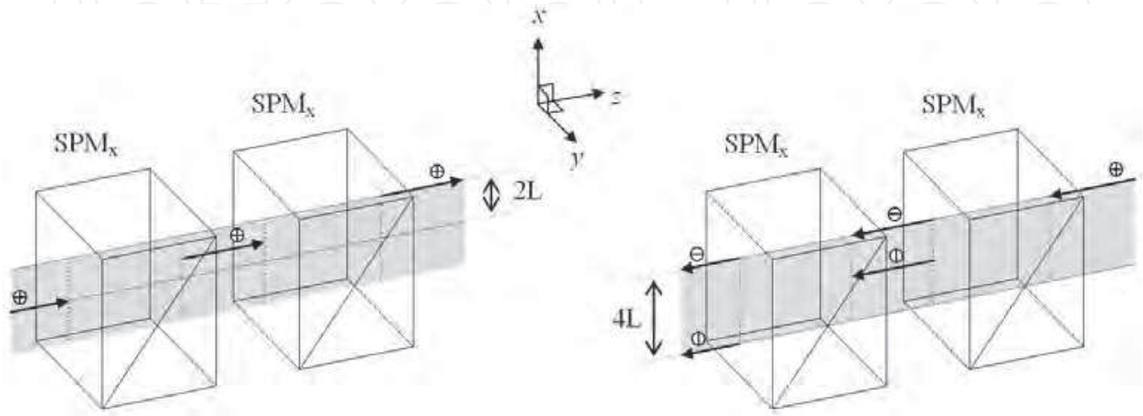


(a) (b)

Fig. 9. Structure and operation characteristic of two connected $SPM_x$s for (a) forward and (b) backward transmissions.

In Fig. 9(a), when an unpolarized light is incident into the module in +$z$ direction, the transmitted unpolarized light is spatially shifted 2$L$ in +$x$ direction. On the other hand, Fig. 9(b) shows that when an unpolarized light is incident into the module in −$z$ direction, the $h$-polarized light transmits the module directly and the $v$-polarized light transmits the module with a lateral shift 4$L$ in −$x$ direction. Consequently, Fig. 10 shows that when an unpolarized light is shuttled between the two sides of the module, the $h$- and $v$-polarized components are separated in two opposite directions gradually in $x$-$z$ plane at $y$=0. The corresponding $x$ coordinates of the $h$- and $v$-polarized components at two sides of the module can be expressed as

$$\begin{bmatrix} x_{h(2n-1)} \\ x_{v(2n-1)} \end{bmatrix} = \begin{bmatrix} 2(n-1)L \\ 2(1-n)L \end{bmatrix}, \text{ (for an odd port)} \tag{11}$$

and

$$\begin{bmatrix} x_{h(2n)} \\ x_{v(2n)} \end{bmatrix} = \begin{bmatrix} 2nL \\ 2(2-n)L \end{bmatrix}, \text{ (for an even port)} \tag{12}$$

where subscripts $h$ and $v$ denote the $h$- and $v$-polarized components, (2$n$-1) and (2$n$) indicate the port numbers, and $n$ is a positive integer. Accordingly, the module can sequentially guide and separate the forward and backward transmitted lights in a z-shape.

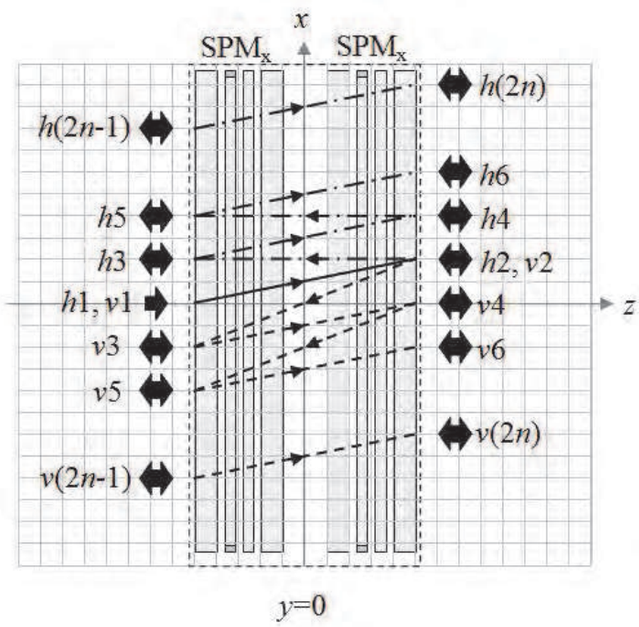


Fig. 10. Operation characteristic for an unpolarized light shuttled between the two sides of two connected $SPM_x$s.

### 3.1.2 Orthogonal connection of two SPMs

Similarly, as shown in figures 11(a) and 11(b), a $SPM_y$ and a $SPM_x$ are sequentially connected, *i.e.* orthogonal connection of two SPMs. In Fig. 11(a), when an unpolarized light is incident into the module in $+z$ direction, the transmitted unpolarized light is spatially shifted $L$ in $+x$ and $-y$ directions, respectively. On the other hand, Fig. 11(b) shows that when an unpolarized light is incident into the module in $-z$ direction, the $h$-polarized light transmits the module with a lateral shift $2L$ in $+y$ direction and the $v$-polarized light transmits the module with a lateral shift $2L$ in $-x$ direction. Consequently, Fig. 12 shows that when an unpolarized light is shuttled between the two sides of the module, the $h$- and $v$-polarized components are separated in two opposite directions gradually along two slanted lines $y=x$ and $y=x-2$, respectively. The corresponding $(x, y)$ coordinates of the $h$- and $v$-polarized components at two sides of the module can be expressed as

$$\begin{bmatrix} x_{h(2n-1)} & y_{h(2n-1)} \\ x_{v(2n-1)} & y_{v(2n-1)} \end{bmatrix} = \begin{bmatrix} (n-1)L & (n-1)L \\ (1-n)L & (1-n)L \end{bmatrix}, \text{ (for an odd port)} \tag{13}$$

and

$$\begin{bmatrix} x_{h(2n)} & y_{h(2n)} \\ x_{v(2n)} & y_{v(2n)} \end{bmatrix} = \begin{bmatrix} nL & (n-2)L \\ (2-n)L & -nL \end{bmatrix}. \text{ (for an even port)} \tag{14}$$

Accordingly, the module can sequentially guide and separate the forward and backward transmitted lights in another z-shape.

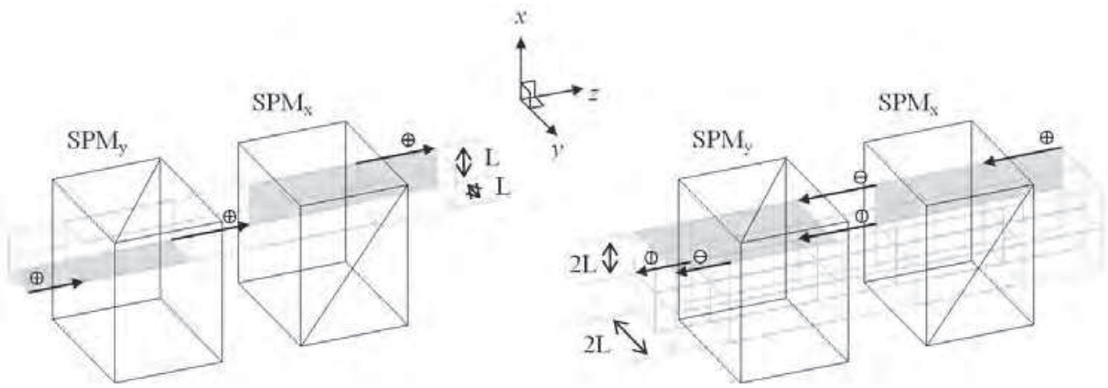


(a) (b)

Fig. 11. Structure and operation characteristic of the connected $SPM_y$ and $SPM_x$ for (a) forward and (b) backward transmissions.

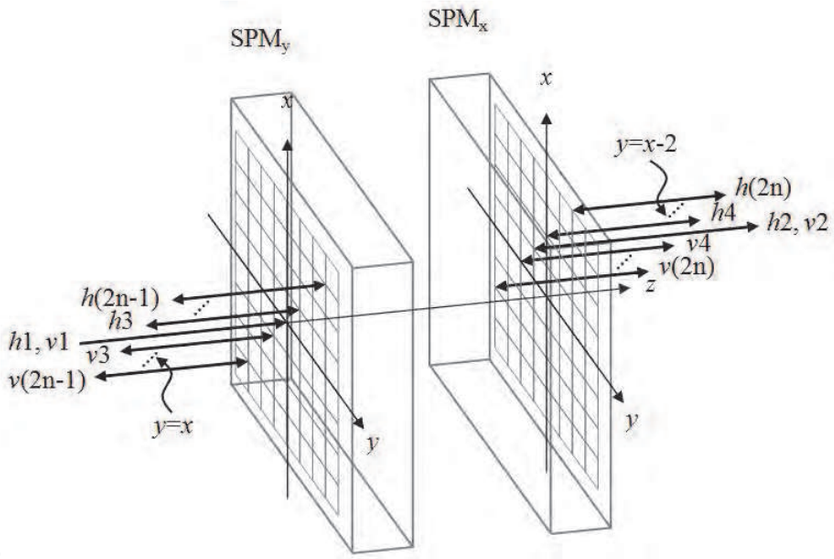


Fig. 12. Operation characteristic for an unpolarized light shuttled between the connected $SPM_y$ and $SPM_x$.

### 3.2 Four-port polarization-independent optical circulator

Shown in Fig. 13 is the design of proposed holographic-type 4-port polarization-independent optical circulator. In the design, based on a previously described SPM, two polarization-selective substrate-mode volume holograms are applied to implement the function of spatial walk-off polarizers. They are consequently termed as holographic spatial walk-off polarizers (HSWPs). The two identical HSWPs face the opposite directions as shown in the figure. Besides the SPM, this optical circulator also consists of four reflection prisms (RPs) and six polarization-beam splitters (PBSs). If an input beam is normally incident on $HSWP_1$ from Port 1, as shown in Fig. 13(a), then the *s*- polarized component passes through $HSWP_1$ directly and the *p*- polarized component also passes through $HSWP_1$

after two diffractions and two total internal reflections. Next, these two orthogonally polarized components pass through FR and H. Their state of polarization (SOP) are rotated a total of 90°, +45° by FR and +45° by H. For easy understanding, a circle with a bisecting line is used to represent the associated SOP of the light after propagating through each component. Symbols ⦶ and ⊖ represent the electric field lies in the planes perpendicular (*s*-polarization) and parallel (*p*-polarization) to the paper plane respectively, and the symbol ⊕ represents the light beam has both *s*- and *p*-polarized components. The beams finally enter $HSWP_2$ and then recombine together with the similar diffraction and total internal reflection effects in $HSWP_1$ and reach Port 2.

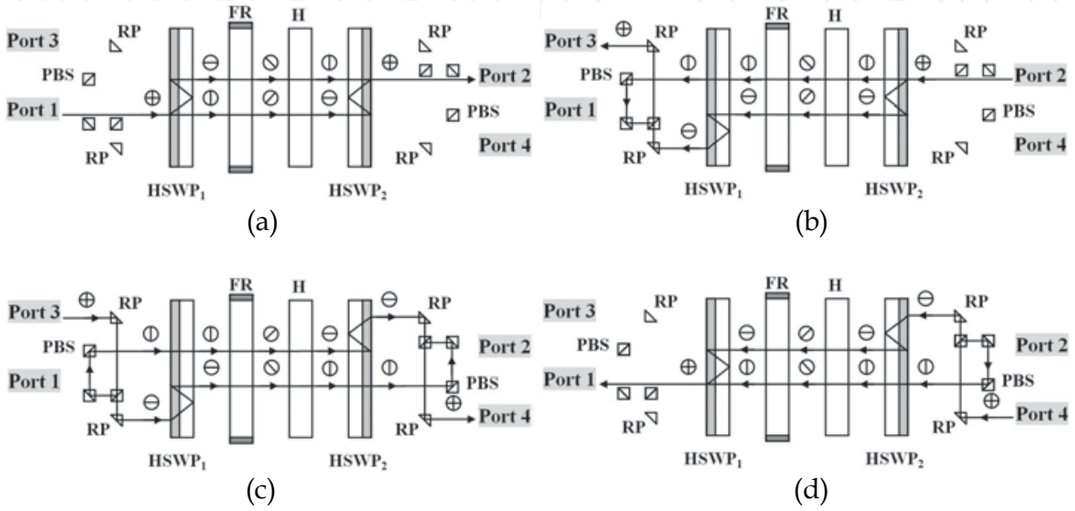


Fig. 13. Structure and operation principles of the 4-port polarization independent optical circulator.

On the other hand, if an input beam is incident normally on $HSWP_2$ from Port 2 as shown in Fig. 13(b), then the *s*-polarized component passes through $HSWP_2$ directly, and the *p*-polarized component also passes through $HSWP_2$ after two diffractions and two total internal reflections. These two orthogonally polarized components pass through H and FR. Their SOPs are rotated -45° by H and +45° by FR, a total of 0°. The *s*-polarized component passes through $HSWP_1$ and is reflected by three PBSs and one PR, and enters Port 3. The *p*-polarized component is diffracted and total internal reflected similarly in $HSWP_1$ and propagates through one RP, one PBS, and another RP. Finally, it arrives at Port 3 and recombines with the *s*-polarized component. Two other similar operations for the routes of Port 3→Port 4 and Port 4→Port 1 can be done with the introduction of additional RPs and PBSs, as shown in Fig. 13(c) and 13(d) respectively.

If the PBSs are located accurately in the configurations of Fig. 13(b) and 13(d), there will be no optical path difference between *s*- and *p*-polarizations for any route. Hence, this optical circulator can function as a polarization-independent 4-port optical circulator without polarization mode dispersion (PMD).

Listed in Table 3 are parameters for a prototype of 4-port optical circulator which were estimated from the diffraction efficiencies of fabricated HSWPs and the transmittances of FR and H. The diffraction efficiencies of $\eta_s$ and $\eta_p$ are 3% and 90%, respectively; the transmittances of FR and H are 0.95 and 0.97, respectively. Because $\eta_s$ and $\eta_p$ are slightly

different from theoretical values, the transmittances of two orthogonally polarized components are slightly different in the routes of Port 2→Port 3 and Port 4→Port 1.

| | Out Port | | | |
|---|---|---|---|---|
| In Port | 1 | 2 | 3 | 4 |
| 1 | 14.26[a] | 2.09[b] | 47.91[c] | 14.18[c] |
| 2 | 11.91[c] | 14.26[a] | 2.02[b] | 47.91[c] |
| 3 | 28.24[c] | 14.15[c] | 14.26[a] | 2.09[b] |
| 4 | 2.02[b] | 28.24[c] | 44.92[c] | 14.26[a] |

Table 3. Associated parameters (in Decibels) for the prototype 4-port optical circulator with wavelength 1300 nm; [a]Return losses; [b]Insertion losses; [c]Isolations.

Since the fabricated HSWPs have no anti-reflection coatings, there is about 4% reflection loss at each boundary. If they are anti-reflection coated, then the reflection losses should be decreased to 0.1%. In addition, if the holographic exposure and the post-processing procedure are controlled more accurately, the HSWPs may have the theoretical diffraction efficiencies, i.e., $\eta_s \cong 0\%$ and $\eta_p \cong 100\%$. Under these two possible improved conditions, the performance of this 4-port optical circulator can be enhanced greatly for demands of a commercial device. Moreover, if $K$ and $\Delta\lambda$ are the magnitude of grating vector $\vec{K}$ and the wavelength shift with respect to the central wavelength $\lambda_r$, the diffraction efficiencies of a transmission-type phase volume hologram for the *s*- and *p*-polarization states near the Bragg condition are given as [Kogelnik, 1969]

$$\eta_i = \frac{\sin^2(\sqrt{\nu_i^2 + \xi^2})}{(1 + \xi^2 / \nu_i^2)} \quad (i = s, p), \tag{15}$$

with

$$\xi = \frac{-\Delta\lambda K^2 d}{8\pi n_{f2} \cos\theta_d}, \tag{16a}$$

$$K = (\frac{4\pi n_{f2}}{\lambda_r}) \cdot \sin\frac{\theta_d}{2}. \tag{16b}$$

Substituting the experimental conditions $n_1$=0.054, $d$=17μm, $\lambda_r$=1300nm, $\theta_{r2}$=60°, and $n_{f2}$=1.48 (at $\lambda_r$=1300nm) into eq. (15), the theoretical curves of diffraction efficiencies versus wavelengths for the HSWP is shown in Fig. 14. It is obvious that the bandwidth with $\eta_p$>90% and $\eta_s \cong 0\%$ at 1300nm central wavelength is as large as 20nm. It is also possible to design the central wavelength at other ranges for optical communications.

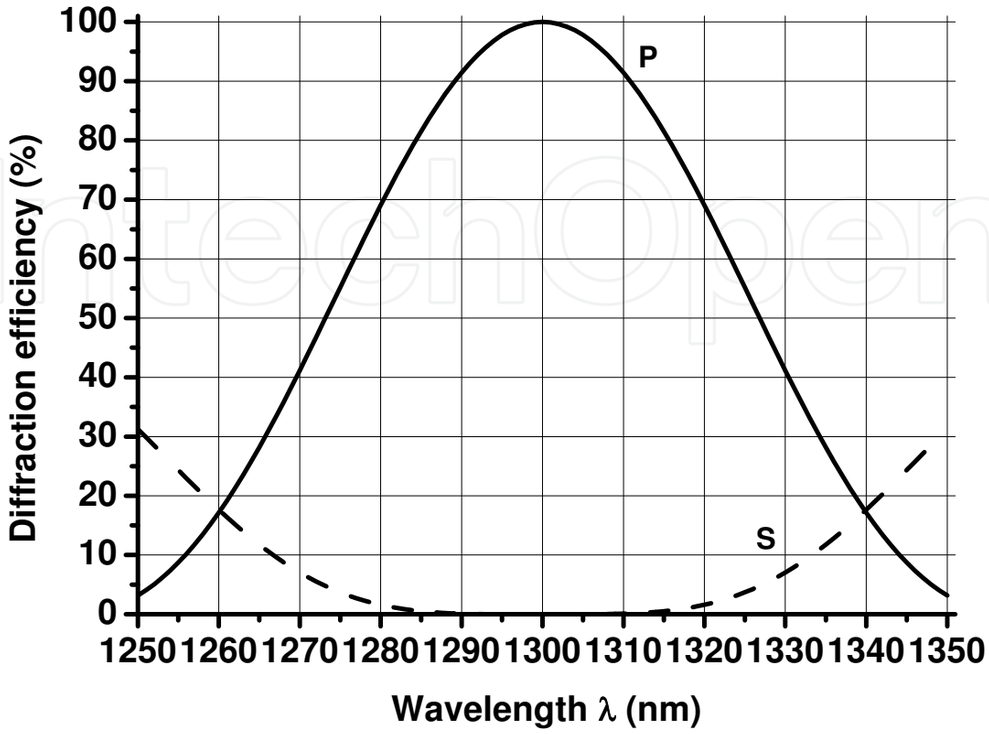


Fig. 14. Calculated diffraction efficiencies of the HSWP versus wavelength at 1300 nm central wavelength.

### 3.3 Multi-port polarization-independent optical quasi-circulator

Based on two connected $SPM_x$s, it is obvious that if some polarization-beam splitters (PBSs), and reflection prisms (RPs) are introduced appropriately at the corresponding positions of the *h*- and *v*-components, a multi-port optical quasi-circulator can be obtained. Shown in Fig. 15 is an optical quasi-circulator with 2n-ports consisting of a pair of $HSPM_x$s, PBSs, and RPs. According to equations (11) and (12), the introduced PBSs and RPs at the *j*-th port are located at $(x_{PBSj}, z_{PBSj})$ and $(x_{RPj}, z_{RPj})$, which can be expressed as

$$\begin{bmatrix} x_{PBS(2n-1)} & z_{PBS(2n-1)} \\ x_{RP(2n-1)} & z_{RP(2n-1)} \end{bmatrix} = \begin{bmatrix} 2(n-1)L & (-2n-4)L \\ 2(1-n)L & (-2n-4)L \end{bmatrix}, \text{ (for an odd port)} \tag{17}$$

$$\begin{bmatrix} x_{PBS(2n)} & z_{PBS(2n)} \\ x_{RP(2n)} & z_{RP(2n)} \end{bmatrix} = \begin{bmatrix} 2nL & (2n+4)L \\ 2(2-n)L & (2n+4)L \end{bmatrix}, \text{ (for an even port)} \tag{18}$$

where *n* is a positive integer. Figure 15(a), (b), (c), and (d) show the routes of port 1→port 2, port 2→port 3, port 3→port 4, and port (2n-1)→port 2n, respectively. In these figures, symbols ◪ and ◢ represent a PBS and a RP. Other propagation routes can be obtained based on the similar principle.

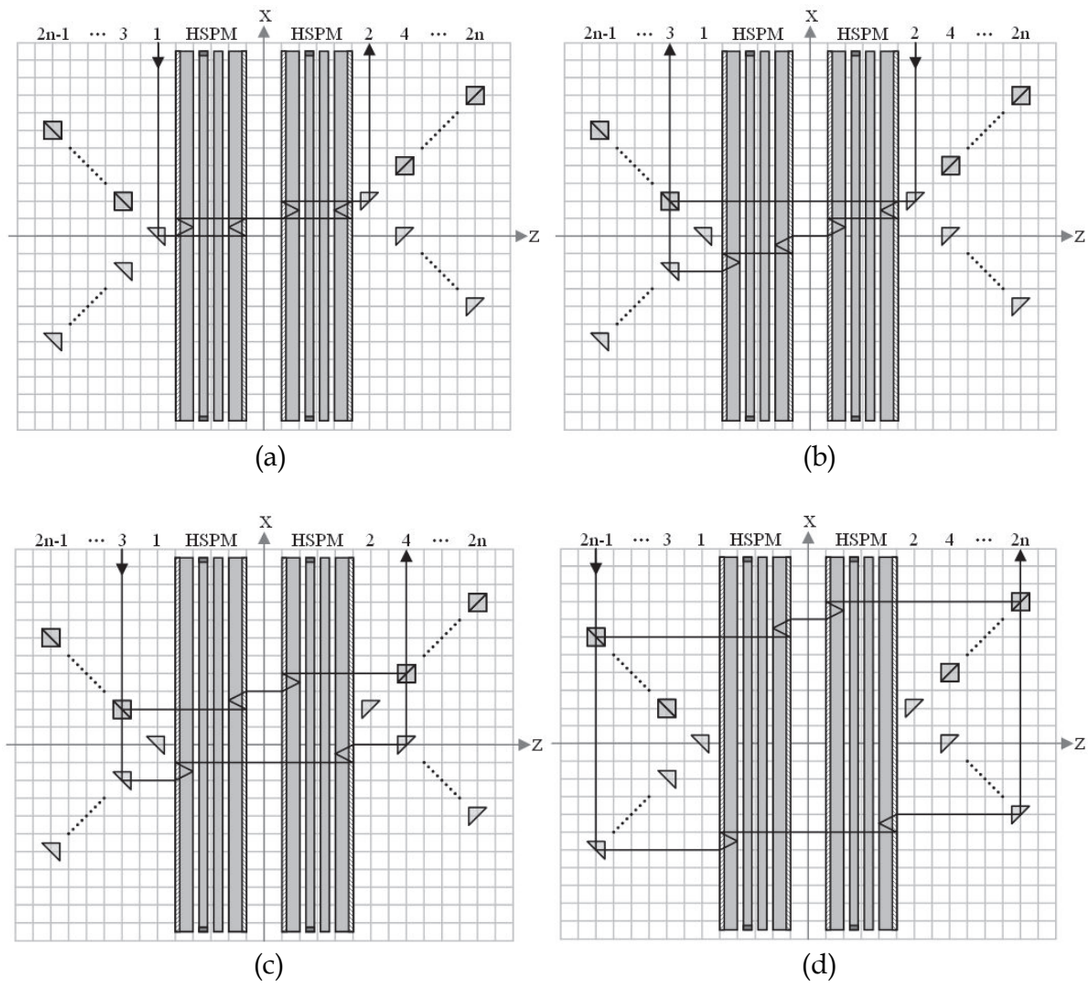


Fig. 15. Structure and operation principles of the proposed multi-port optical quasi-circulator.

However, in the design of Fig. 15, the optical path of the *p*- component is larger than that of the *s*-component. This optical path difference might cause polarization mode dispersion (PMD) to blur the transmission signal. Therefore, in order to solve the PMD problem, the original optical guiding paths in Fig. 15 must be changed. As shown in Fig. 16, two different guiding modules can be introduced for the odd and even ports, respectively, which are composed of PBSs and RPs. The designs of these two guiding modules with specifications (*Length*×*Width*) of (4*n*-3)*L*×0.31(*n*-1)*L* and (4*n*-4)*L*×0.31(*n*-1)*L* for an odd and an even port are shown in Fig. 17(a) and (b), respectively. These guiding modules are located at ($x_{Mj}$, $z_{Mj}$) which can be expressed as

$$[x_{M(2n-1)} \quad z_{M(2n-1)}] = [2(1-n)L \quad (-2n-4)L], \text{ (for an odd port)} \tag{19}$$

$$[x_{M(2n)} \quad z_{M(2n)}] = [2nL \quad (2n+4)L], \text{ (for an even port)} \tag{20}$$

where $n$ is a positive integer larger than 1. The coordinate in equation (19) corresponds to the center of the RP (in red color) in the odd-port guiding module; the coordinate in equation (20) corresponds to the center of the PBS (in green color) in the even-port guiding module. When the guiding modules are appropriately introduced, the optical path differences between the $h$- and $v$-components can be reduced to zero. Therefore, the PMD problem can be solved. Fig. 16(a), (b), (c), and (d) show the routes of port 1→port 2, port 2→port 3, port 3→port 4, and port (2n-1)→port 2n, respectively. Other propagation routes can be obtained based on the similar principle.

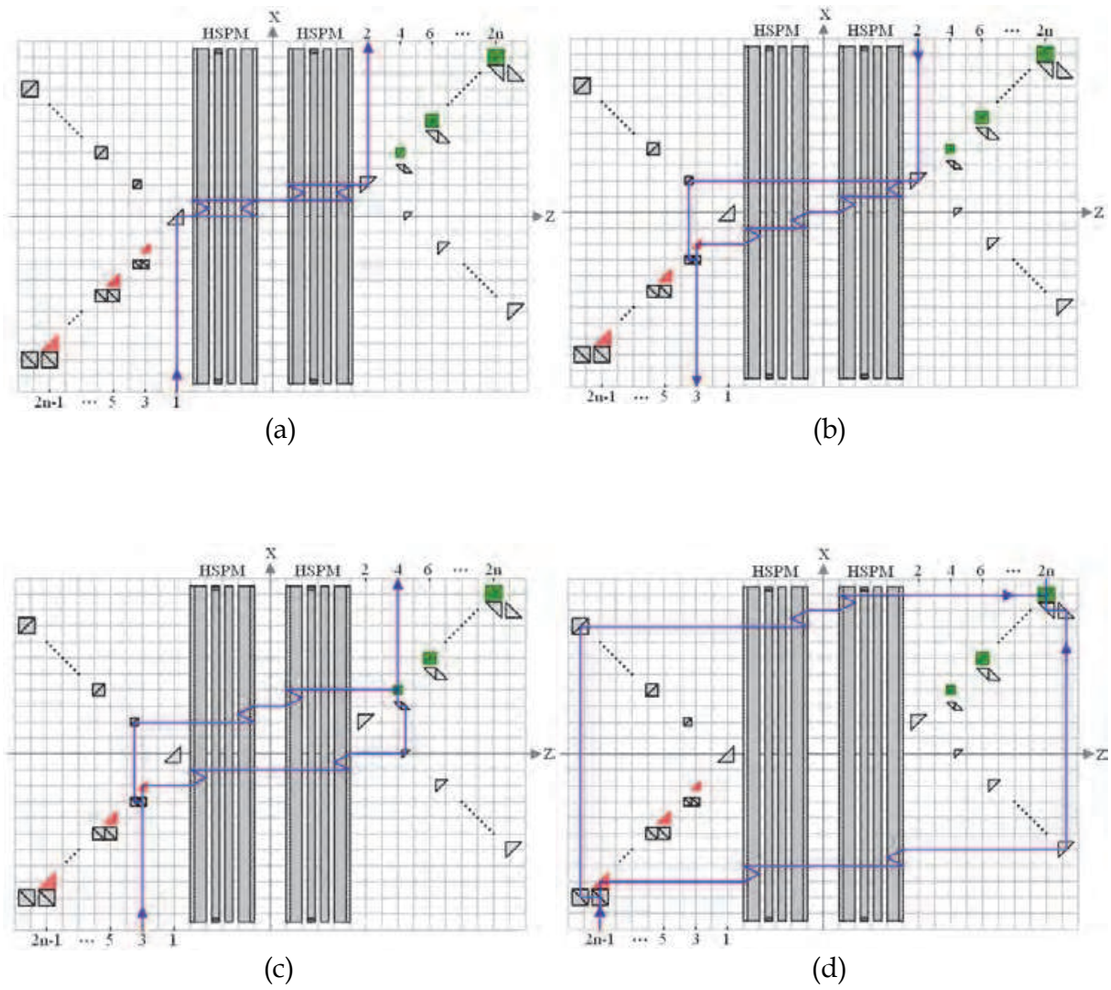


Fig. 16. Structure and operation principles of the proposed multi-port optical quasi-circulator without polarization mode dispersion.

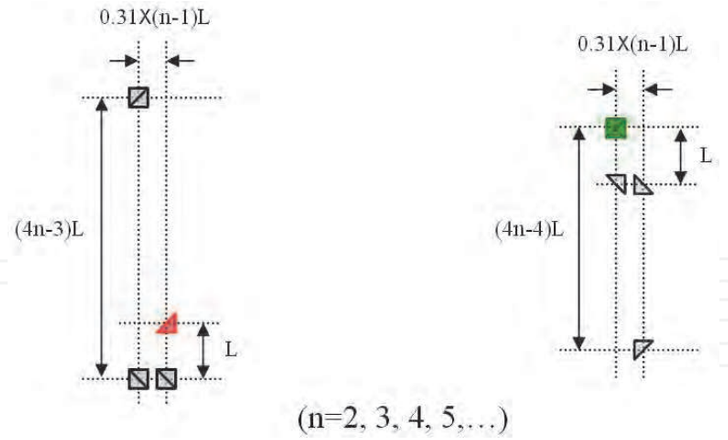


Fig. 17. PBSs and RPs guiding modules for (a) the odd ports; (b) the even ports.

Use the fabricated HSWPs mentioned in Section 3.2, a prototype of 6-port polarization-independent optical quasi-circulator for 1300nm can be assembled. In addition to a pair of HSPMs, it needs another eight polarization-beam splitters and ten reflection prisms to complete the function of this 6-port optical quasi-circulator. The characteristic parameters of this prototype device are estimated and listed in Table 4.

| | Out Port | | | | | |
|---|---|---|---|---|---|---|
| In Port | 1 | 2 | 3 | 4 | 5 | 6 |
| 1 | 14.26[a] | 4.18[b] | >25.36[c] | >25.36[c] | >25.36[c] | >25.36[c] |
| 2 | >26.92[c] | 14.26[a] | 3.90[b] | >26.92[c] | >26.92[c] | >26.92[c] |
| 3 | >25.36[c] | >25.36[c] | 14.26[a] | 4.18[b] | >25.36[c] | >25.36[c] |
| 4 | >26.92[c] | >26.92[c] | >26.92[c] | 14.26[a] | 3.90[b] | >26.92[c] |
| 5 | >25.36[c] | >25.36[c] | >25.36[c] | >25.36[c] | 14.26[a] | 4.18[b] |

Table 4. Associated parameters (in Decibels) for the prototype 6-port optical quasi-circulator with wavelength 1300 nm; [a]Return losses; [b]Insertion losses; [c]Isolations.

In order to solve the PMD problem, two different guiding modules composed of PBSs and RPs can be appropriately introduced for the odd and even ports, respectively. However, if more compact modules are desired, these guiding devices should become smaller simultaneously. The result will increase the difficulty of device assembling. Expediently, we can increase the beam splitting distance L ($L$=2$t$tan$\theta_d$) by increasing the thickness of the substrate to reduce the assembling difficulty. Another reliable method is to operate this device beginning with a high number port.

### 3.4 Improved multi-port polarization-independent optical quasi-circulator

Based on two connected $SPM_y$ and $SPM_x$, it is obvious that if reflection prisms (RPs) and polarization beam-splitters (PBSs) are introduced appropriately to guide the light beams in and out of the module, an alternative multi-port optical quasi-circulator can also be obtained. Only one RP should be added at port 1 and port 2, separately. For other ports, each port needs two RPs and one PBS. According to eqs. (13) and (14), the introduced RPs and PBS at the $j$-th port are located at ($x_{RP1j}$, $y_{RP1j}$), ($x_{RP2j}$, $y_{RP2j}$) and ($x_{PBSj}$, $y_{PBSj}$), which can be expressed as

$$\left[\begin{matrix} x_{RP1(2n-1)} & y_{RP1(2n-1)} \\ x_{RP2(2n-1)} & y_{RP2(2n-1)} \\ x_{PBS(2n-1)} & y_{PBS(2n-1)} \end{matrix}\right]_{z=-L} = \left[\begin{matrix} (n-1)L & (1-n)L \\ (1-n)L & (n-1)L \\ (n-1)L & (n-1)L \end{matrix}\right]_{z=-L}, \text{ (for an odd port)} \quad (21)$$

$$\left[\begin{matrix} x_{RP1(2n)} & y_{RP1(2n)} \\ x_{RP2(2n)} & y_{RP2(2n)} \\ x_{PBS(2n)} & y_{PBS(2n)} \end{matrix}\right]_{z=L} = \left[\begin{matrix} nL & (2-n)L \\ (2-n)L & nL \\ nL & nL \end{matrix}\right]_{z=L}, \text{ (for an even port)} \quad (22)$$

These equations are still valid for port 1 and port 2 to determine the position of its associated RP. Shown in Fig. 18 is a 5-port polarization-independent optical quasi-circulator consisting of a pair of $HSPM_x$ and $HSPM_y$, 3 PBSs, and 8 RPs. Figures 18(a) and 18(b) show the routes of port 1→port 2 and port 4→port 5, respectively. Based on the same principle, other propagation and expanded routes can also be obtained.

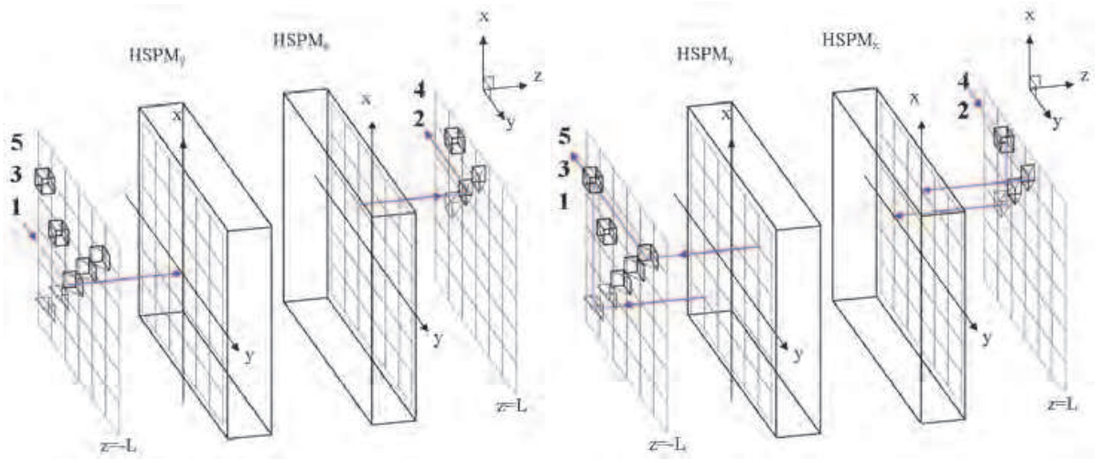


(a) (b)

Fig. 18. Structure and operation principles of the proposed 5-port polarization-independent optical quasi-circulator.

A 5-port polarization-independent optical quasi-circulator for 1300nm can be assembled with the fabricated HSWPs. In addition to a pair of orthogonal HSPMs, it needs another three PBSs and eight RPs to complete the function of this device. Its associated losses and isolation values are estimated and listed in Table 5. The isolation values are in the range from 20 to 54dB. The return losses and the insertion losses are about 14dB and about 3dB, respectively. Return losses mainly come from the interface reflections that influence the isolation values directly. If the applied HSWPs are anti-reflection coated and are fabricated under accurate fabrication processes, the return losses could be over 50 dB and the diffraction efficiencies may reach theoretical values, i.e., $\eta_h$=0% and $\eta_v$=100%. Under these two improved conditions, the performance of this 5-port optical quasi-circulator can be enhanced greatly with isolation values larger than 51dB and insertion losses smaller than 0.9dB.

| | Out Port | | | | |
|---|---|---|---|---|---|
| In Port | 1 | 2 | 3 | 4 | 5 |
| 1 | 14.26[a] | 3.26[b] | >20.46[c] | >37.65[c] | >54.85[c] |
| 2 | >54.85[c] | 14.26[a] | 3.26[b] | >20.46[c] | >37.65[c] |
| 3 | >37.65[c] | >54.85[c] | 14.26[a] | 3.26[b] | >20.46[c] |
| 4 | >54.85[c] | >54.85[c] | >54.85[c] | 14.26[a] | 3.26[b] |

Table 5. Associated parameters (in Decibels) for the prototype 5-port optical quasi-circulator with wavelength 1300 nm; [a]Return losses; [b]Insertion losses; [c]Isolations.

Compared with the design in Section 3.3, only the second HSPM is rotated 90° clockwise in this improved device. So this design still has all the advantages of the previous one. In addition, because two orthogonally polarized components have the same numbers of diffractions and total internal reflections in this design, their optical path lengths are all the same. Consequently, only fewer PBSs and RPs are required to guide the light beams in and out of the module. Hence the optical configuration is simpler and it is easier to be assembled. Moreover, the optical paths and the optical elements are not restricted in the same plane as the previous design in Section 3.3. So the light leakages producing by the unideal diffraction efficiencies of the HSWPs can not enter any port. The crosstalk between any ports can be avoided. Hence this design has higher isolations. In this device, polarization-selective substrate-mode volume holograms are used to replace conventional crystal spatial walk-off polarizers. Accordingly, compared with conventional quasi-circulators, this design has merits of compactness, easy fabrication, and low-cost. So it has high potential in optical communications.

## 4. Conclusion

In this chapter, polarization-selective substrate-mode volume holograms were introduced which are applied in several novel designs of optical circulator. Alternative design method of polarization-selective substrate-mode volume holograms was also introduced for overcoming the finite refractive index limit in practical holographic recording materials. The described optical circulators have advantages of polarization-independent, compactness, high isolation, low polarization mode dispersion, easy fabrication, and low cost. In addition, the port number of the proposed multi-port device can be expanded easily. High application potential of these devices in optical communications is expected. Their commercialization finally relies on available high-performance holographic recording materials.

## 5. Acknowledgment

These researches were supported partially by grants from the National Science Council, Taiwan, ROC, under contracts NSC 94-2215-E-035-003, NSC 94-2215-E-035-009, NSC 96-2221-E-035-052, NSC 97-2221-E-035-016-MY3, and the Lee & MTI Center for Networking at National Chiao Tung University, Taiwan, ROC.

## 6. References

Ramaswami, R.; Sivarajan, K.; & Sasaki, G. (2009). Optical Networks: A Practical Perspective. 3rd ed. Morgan Kaufmann, ISBN 9780123740922, San Francisco, USA

Hecht, J. (2005). Understanding fiber optics. 5th ed. Prentice Hall, ISBN 9780131174290, New Jersey, USA

Mynbaev, D. & Scheiner, L. (2000). Fiber-Optic Communications Technology. Prentice Hall, ISBN 9780139620690, New Jersey, USA

Iwamura, H. et al. (1997). Simple polarisation-independent optical circulator for optical transmission systems. *Electronics Letters*, Vol. 15, pp. 830-831

Shirasaki, M. et al. (1981). Compact polarization-independent optical circulator. *Applied Optics*, Vol. 20, pp. 2683-2687

Yokohama, I. et al. (1986). Polarisation-independent optical circulator consisting of two fibre-optic polarising beam splitters and two YIG spherical lenses. *Electronics Letters*, Vol. 22, pp. 370-372

Koga, M. (1994). Compact quartzless optical quasi-circulator. *Electronics Letters*, Vol. 30, pp. 1438-1440

Wang, L. (1998). High-isolation polarization-independent optical quasi-circulator with a simple structure. *Optics Letters*, Vol. 23, pp. 549-551

Nicholls, J. (2001). Birefringent crystals find new niche in WDM networks. *WDM Solutions*, R&D Review 2001, pp. 33-36

Huang, Y. (1994). Polarizing-selective volume holograms: general design. *Applied Optics*, Vol. 33, pp. 2115-2120

Chen, J. et al. (2003) Holographic spatial walk-off polarizer and its application to a 4-port polarization-independent optical circulator. *Optics Express*, Vol. 11, pp. 2001-2006

Chen, J. et al. (2008) An alternative design of holographic polarization-selective elements. *Proceedings of SPIE*, Vol. 7072 , pp. 707210-1, San Diego, California, USA

Chen, J. et al. (2004). Multi-port polarization-independent optical circulators by using a pair of holographic spatial- and polarization- modules. *Optics Express*, Vol. 12, pp. 601-608

Chen, J. et al. (2004). Improved N-port optical quasi-circulator by using a pair of orthogonal holographic spatial- and polarization- modules. *Optics Express*, Vol. 12, pp. 6553-6558

Kogelnik, H. (1969). Coupled wave theory for thick hologram gratings. *Bell System Technical Journal*, Vol. 48, pp. 2909-2947

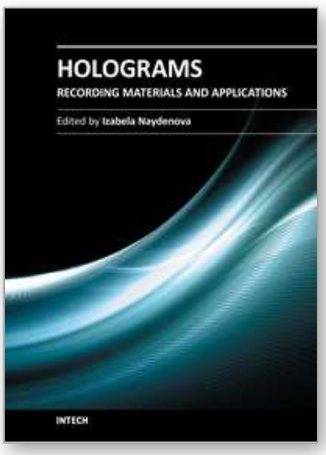


**Holograms - Recording Materials and Applications**

Edited by Dr Izabela Naydenova

ISBN 978-953-307-981-3
Hard cover, 382 pages
**Publisher** InTech
**Published online** 09, November, 2011
**Published in print edition** November, 2011

Holograms - Recording Materials and Applications covers recent advances in the development of a broad range of holographic recording materials including ionic liquids in photopolymerisable materials, azo-dye containing materials, porous glass and polymer composites, amorphous chalcogenide films, Norland optical adhesive as holographic recording material and organic photochromic materials. In depth analysis of collinear holographic data storage and polychromatic reconstruction for volume holographic memory are included. Novel holographic devices, as well as application of holograms in security and signal processing are covered. Each chapter provides a comprehensive introduction to a specific topic, with a survey of developments to date.

**How to reference**

In order to correctly reference this scholarly work, feel free to copy and paste the following:

Jing-Heng Chen, Kun-Huang Chen and Der-Chin Su (2011). Polarization-Selective Substrate-Mode Volume Holograms and Its Application to Optical Circulators, Holograms - Recording Materials and Applications, Dr Izabela Naydenova (Ed.), ISBN: 978-953-307-981-3, InTech, Available from: http://www.intechopen.com/books/holograms-recording-materials-and-applications/polarization-selective-substrate-mode-volume-holograms-and-its-application-to-optical-circulators

INTECH
open science | open minds

**InTech Europe**
University Campus STeP Ri
Slavka Krautzeka 83/A
51000 Rijeka, Croatia
Phone: +385 (51) 770 447
Fax: +385 (51) 686 166
www.intechopen.com

**InTech China**
Unit 405, Office Block, Hotel Equatorial Shanghai
No.65, Yan An Road (West), Shanghai, 200040, China
中国上海市延安西路65号上海国际贵都大饭店办公楼405单元
Phone: +86-21-62489820
Fax: +86-21-62489821

IntechOpen